Quantum phases of the Shastry-Sutherland antiferromagnet: Application to $SrCu_2(BO_3)_2$

C. H. Chung and J. B. Marston
Department of Physics, Brown University, Providence, Rhode Island 02912-1843

Subir Sachdev
Department of Physics, Harvard University, Cambridge, Massachusetts 02138
and Department of Physics, Yale University, P.O. Box 208120, New Haven, Connecticut 06520-8120

(Received 11 March 2001; published 4 September 2001)

We study possible paramagnetic phases of antiferromagnets on the Shastry-Sutherland lattice by a gauge-theoretic analysis of fluctuations in a theory with $Sp(2N)$ symmetry. In addition to the familiar dimer phase, we find a confining phase with plaquette order and a topologically ordered phase with deconfined $S=1/2$ spinons and helical spin correlations. The deconfined phase is contiguous to the dimer phase and in a regime of couplings close to those found in the insulator $SrCu_2(BO_3)_2$. We suggest that a superconductor obtained by doping this insulator with mobile charge carriers will be an attractive candidate for observing the anomalous magnetic flux properties associated with topological order.

DOI: 10.1103/PhysRevB.64.134407 PACS number(s): 75.10.Jm, 75.30.Kz

I. INTRODUCTION

Much interest has recently focused on the magnetic properties of the insulator $SrCu_2(BO_3)_2$.[1,2] The low-energy spin excitations in this material reside on the $S=1/2$ Cu ions which lie in two-dimensional layers decoupled from each other. The experiments show a clear indication of an energy gap towards spin excitations, making this one of the few known two-dimensional systems with a spin gap. Remarkably, the pattern of near-neighbor antiferromagnetic exchange couplings between the Cu ions turns out to be identical to that in a model Hamiltonian studied many years ago by Shastry and Sutherland.[3] These authors also showed that a simple decoupled dimer wave function was an exact eigenstate of this Hamiltonian and that it was the ground state over a restricted parameter regime.

The Shastry-Sutherland antiferromagnet is sketched in Fig. 1. The Hamiltonian is

$$H=J_1\sum_{\langle ij\rangle}\mathbf{S}_i\cdot\mathbf{S}_j+J_2\sum_{\text{diagonals}}\mathbf{S}_i\cdot\mathbf{S}_j\,, \tag{1.1}$$

where $\mathbf{S}_i$ are $S=1/2$ operators on the sites i of a square lattice. The exchange $J_1>0$ acts along the nearest-neighbor links (shown as solid lines in Fig. 1), while $J_2>0$ acts on the diagonal links, shown as dashed in lines in Fig. 1. It was established[3] that a simple product of singlet pairs on the diagonal links was the ground state of H for sufficiently large J_2/J_1. However, an understanding of the experiments requires a description of the excitation spectrum and also of possible quantum phase transitions to other states at smaller J_2/J_1. These issues have been addressed in a number of recent theoretical works.[4–11] Many of these studies[4,6–8] involve numerical analyses based upon large-order series expansions departing from various decoupled cluster states. Quantum Monte Carlo simulations have, in principle, a smaller bias due to the choice of an initial state and can be extended to much larger system sizes; however, simulations of H suffer from a sign problem, and so such studies have not been possible. An analytic Schwinger boson mean-field approach was undertaken by Albrecht and Mila:[5] Results were obtained mainly for the magnetically ordered states, and the various distinct paramagnetic states were not distinguished.

Quite apart from determining the ground states of the specific Hamiltonian H, it is also of interest to determine the phases of models which are ''near'' the parameter space of H. This is in the hope that future experiments may succeed in deforming the insulator $SrCu_2(BO_3)_2$ by substitutional doping (which can induce mobile carriers) or by the application of hydrostatic pressure. Doping the antiferromagnetic insulator La_2CuO_4 led to the discovery of high-temperature superconductivity: Related phenomena may be expected here, although, as we shall argue later, the presence of strong frustration in the parent insulator $SrCu_2(BO_3)_2$ may lead to profound differences in the nature of a possible superconducting ground state.

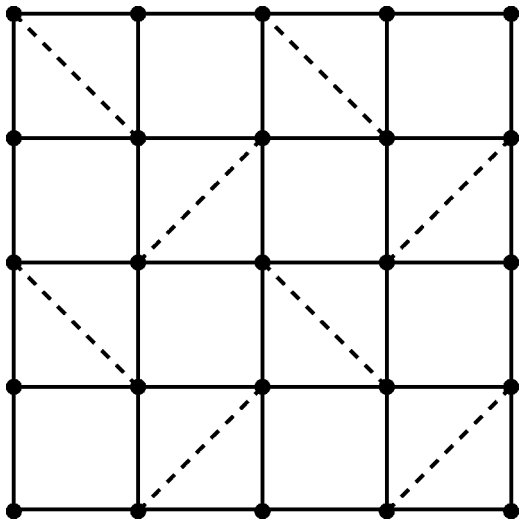

FIG. 1. The Shastry-Sutherland lattice. The exchange J_1 acts between sites separated by the horizontal and vertical links, which the exchange J_2 acts across the diagonal links.

This paper will examine a generalization of H to Sp($2N$) symmetry [SU(2)$\cong$Sp(2)] and describe the properties of the large-N limit. Some of the phases obtained in such a large-N limit may not actually appear in the phase diagram of the SU(2) model H—nevertheless, as we have just argued, the phases may still be of relevance to physical systems whose microscopic Hamiltonians are near the parameter space of H. Such an approach has been fruitfully applied to a number of other frustrated quantum antiferromagnets in previous work.[12–16] The method leads to an unbiased selection of possible ground states in the large-N limit, both with and without broken spin rotation symmetry. Moreover, a gauge-theoretic description of the fluctuations about the mean-field solution allows a systematic and reliable assessment of the stability of the various ground states, along with a description of the dynamics of the excitations.

The Sp($2N$) generalization of H is defined by introducing canonical Bose creation operators $b_{i\alpha}^{\dagger}$ on every site i, with $\alpha=1,\ldots,2N$ a Sp($2N$) index. The allowed states in the Hilbert space satisfy the constraint

$$b_{i\alpha}^{\dagger}b_i^{\alpha}=2NS \tag{1.2}$$

on every site i [we follow the convention of summing over all repeated Sp($2N$) indices]; the right-hand side of Eq. (1.2) must be a positive integer, and the values of S are constrained accordingly—for the physical case, $N=1$, S must take half-integral values, as expected. The Hamiltonian is

$$H=-\frac{J_1}{2N}\sum_{\langle ij\rangle}(\mathcal{J}^{\alpha\beta}b_{i\alpha}^{\dagger}b_{j\beta}^{\dagger})(\mathcal{J}_{\gamma\delta}b_i^{\gamma}b_j^{\delta}) -\frac{J_2}{2N}\sum_{\text{diagonals}}(\mathcal{J}^{\alpha\beta}b_{i\alpha}^{\dagger}b_{j\beta}^{\dagger})(\mathcal{J}_{\gamma\delta}b_i^{\gamma}b_j^{\delta}), \tag{1.3}$$

where $\mathcal{J}^{\alpha\beta}=\mathcal{J}_{\alpha\beta}=-\mathcal{J}_{\beta\alpha}$ is the generalization of the antisymmetric ε tensor of SU(2) (i.e., $\mathcal{J}$ contains N copies of ε along its center block diagonal and vanishes elsewhere).

The large-N analysis of a large class of models, of which H is a member, was described with some generality in Sec. II of Ref. 15. We will follow the same method here and so will dispense with the details of the computation. The resulting mean-field phase diagram is shown in Fig. 3 below, as a function of J_2/J_1 and $1/S$ (in the large-N limit, S becomes a continuous real variable). The positions of the various phase boundaries are not expected to be quantitatively accurate for the physical $N=1$ case. However, the general topology of the phase diagram, the nature of the phases and their excitations, and the critical properties of the quantum phase transitions can be reliably described using Fig. 3 as a starting point.

The properties of all the phases in Fig. 3 will be discussed in detail in Sec. II. Here we highlight our main results.

One of the paramagnetic phases has short-range equal-time spin correlations peaked at the wave vector (π,π). [We denote this phase (π,π) short-range ordered (SRO) in Fig. 3; here we are placing the sites on the vertices of a regular square lattice as in Fig. 1 and measuring wave vectors in units of 1/(nearest-neighbor spacing). In the experimental $SrCu_2(BO_3)_2$ system, the positions of the sites are different, and there will be a corresponding transformation in the wave vector dependence of observables.] At the mean-field level, this phase is identical to that found earlier[19,20] on the square lattice with $J_2=0$. However, we will show here that a difference does emerge upon consideration of fluctuations. For $J_2=0$, it was shown[19,20] that Berry phases associated with hedgehog instantons led to columnar spin-Peierls order in the (π,π) SRO phase. Here we show that a closely related analysis for the Shastry-Sutherland lattice leads instead to ''plaquette'' order in this phase. Just such a phase was considered recently by Koga and Kawakami.[8]

Our other results are also associated with a paramagnetic phase. This phase is denoted (π,q) SRO in Fig. 3 and is obtained by a destroying the long-range magnetic order in a helically ordered phase. Equal-time spin correlations show short-range incommensurate order, and the spin structure factor is peaked at the incommensurate wave vector (π,q) (the value of q varies continuously as a function of J_2/J_1). As in previous incommensurate SRO phases found on frustrated square lattice models,[12,14] we argue that the excitations above the ground state are *deconfined spinons* which carry spin $S=1/2$ [for SU(2)]. Also, as in previous work,[12,14] the quantum phase transition between this phase and the (π,π) SRO (plaquette) phase (Fig. 3) is described by theory of a charge-2 Higgs scalar coupled to a compact U(1) gauge field; the deconfinement transition is associated with the condensation of the Higgs field, and the critical properties are those of a Z_2 gauge theory.[21,12–14,22–24] We will also consider here the transition between the deconfined phase and the dimer phase: By a somewhat different analysis, we will show that this transition also reduces to a Z_2 gauge theory description.

II. MEAN FIELD PHASE DIAGRAM

As discussed in Sec. II of Ref. 15, a key quantity determining the nature of the phases is a complex, directed, link field $Q_{ij}=-Q_{ji}$. Operationally, this field is introduced to decouple the quartic boson interactions in H by a Hubbard-Stratonovich transformation. After this decoupling, the effective action contains the terms

$$\mathcal{S}=\int d\tau\sum_{i>j}\frac{J_{ij}}{2}[N|Q_{ij}|^2-Q_{ij}\mathcal{J}_{\alpha\beta}b_i^{\alpha}b_j^{\beta}+\text{H.c.}]+\cdots, \tag{2.1}$$

where τ is imaginary time, $J_{ij}=J_1$ ($J_{ij}=J_2$) on the horizontal and vertical (diagonal) links, and the ellipses represent standard terms which impose the canonical boson commutation relations and the constraint (1.2). It is also clear from the structure of $\mathcal{S}$ that the average value of Q_{ij} satisfies

$$\langle Q_{ij}\rangle=\frac{1}{N}\langle\mathcal{J}^{\alpha\beta}b_{i\alpha}^{\dagger}b_{j\beta}^{\dagger}\rangle. \tag{2.2}$$

For larger values of S, the dynamics of $\mathcal{S}$ requires condensation of the b_i^{α} bosons and hence a nonzero value of

$$x_i^{\alpha}=\langle b_i^{\alpha}\rangle; \tag{2.3}$$

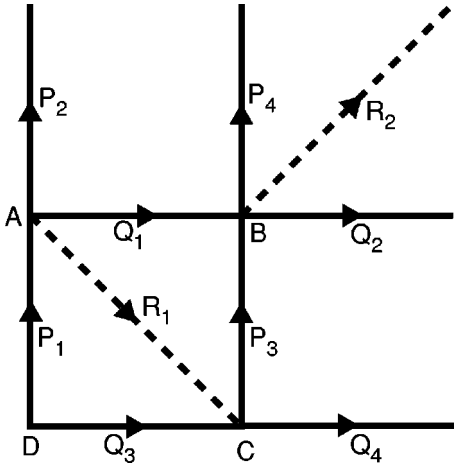

FIG. 2. The four sites of the unit cell (labeled A, B, C, and D), and the ten-link variables Q_{ij}.

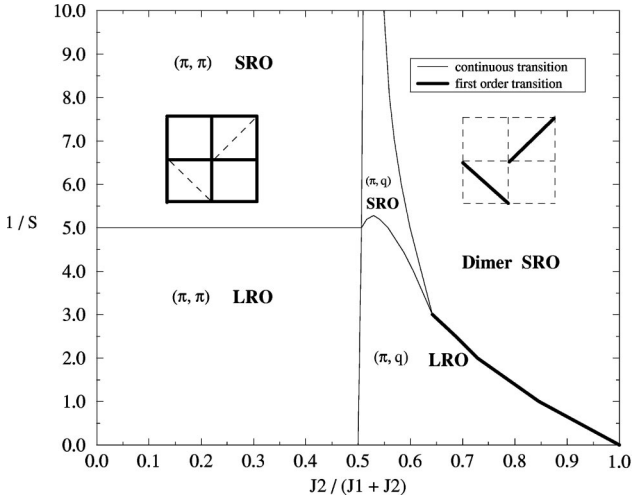

FIG. 3. Large-N phase diagram of the Sp(N) Shastry-Sutherland model, Eq. (1.1), as a function of $J_2/(J_1+J_2)$ and $1/S$. The five phases are described in Sec. II. The LRO phases break spin-rotation symmetry: The spin order is collinear and commensurate in the (π,π) LRO phase and helical and incommensurate in the (π,q) LRO phase. The SRO phases preserve spin-rotation invariance. In the (π,π) SRO only the horizontal and vertical Q_{ij} are nonzero in the large-N theory—fluctuations lead to broken translational symmetry in one of the states shown in Fig. 6. [A state with coexisting (π,π) LRO and plaquette order is also allowed by the theory (Ref. 17) beyond the large-N limit (not shown above), and there is evidence that this occurs on a frustrated square lattice antiferromagnet (Ref. 18).] The dimer phase has only the diagonal Q_{ij} nonzero in the large-N theory. The (π,q) SRO phase has all the Q_{ij} nonzero: This phase has topological order and deconfined spinons.

such phases break the spin rotation symmetry and have magnetic long-range order. As described in Ref 15, we optimized the ground-state energy with respect to variations in $\langle Q_{ij}\rangle$ and x_i^α for different values of J_2/J_1 and S. The four-site unit cell of the Shastry-Sutherland lattice, depicted in Fig. 2, has ten different Q_{ij} fields. Care must be taken to identify gauge-equivalent configurations. We find that each saddle point may be described by purely real $\langle Q_{ij}\rangle$. The resulting phase diagram is shown in Fig. 3. We describe the phases in turn in the following subsections, considering first the magnetically ordered phases with $x_i^\alpha \neq 0$ in Sec. II A and then the paramagnetic phases in Sec. II B.

A. Magnetically ordered phases

1. Néel (π,π) LRO state

This is the familiar long-range-ordered (LRO) state in which $\langle \mathbf{S}_i\rangle$ is collinearly polarized in opposite directions on two checkerboard sublattices. It is known to be the ground state of H for $J_2=0$, $S=1/2$ in the physical $N=1$ limit. A gauge may be chosen in which the expectation values of link variables, $\langle Q_{ij}\rangle$, are nonzero and equal on the horizontal and vertical links, while the expectation values on the diagonal links are zero. In the notation of Fig. 2, then, $Q_i=P_i$ $(i=1,2,3,4)$ and $R_1=R_2=0$.

2. Helical (π,q) and (q,π) LRO states

This phase is characterized by nonzero values of $\langle Q_{ij}\rangle$ on the horizontal, vertical, and diagonal links. A gauge choice sets all the Q_i equal to each other, and similarly for the P_i; in the Appendix we present an argument which shows that the values of the P_i and Q_i are also equal to each other. There are two gauge-nonequivalent choices for the values of $R_{1,2}$: One state has $R_1=R_2$ and the other $R_1=-R_2$. The two states are interchanged under a 90° rotation and correspond to spirals ordered in the horizontal or vertical directions. At large values of the spin, this phase appears at $J_2>J_1$, in accordance with the classical calculation of Shastry and Sutherland.[3] Equal-time spin correlations exhibit long-range incommensurate order, and the spin structure factor peaks at the incommensurate wave vectors (π,q) or (q,π) with the value of q varying continuously as a function of J_2/J_1. This state also appears in the studies of Refs. 5 and 10.

B. Paramagnetic phases

In this subsection we discuss the three phases for which $x_i^\alpha=0$. As a consequence, spin rotation symmetry is preserved and only spin SRO arises; however, there may be ordering in other singlet order parameters.

1. Dimer state

This is the exact SU(2) eigenstate of decoupled singlet pairs found by Shastry and Sutherland.[3] In the large-N limit, this corresponds to a saddle point at which the $\langle Q_{ij}\rangle$ are nonzero only on the diagonal links: $R_1=R_2\neq 0$ and $Q_i=P_i=0$. Note that the b_i^α bosons are spatially decoupled at such a saddle point: Each b_i^α can only hop across a single diagonal link. This simplifies the analysis of fluctuations about the saddle point in or near the dimer state, as will be discussed in Sec. IV. At higher orders in $1/N$, the b_i^α can indeed hop through the entire lattice; we expect that the lowest-lying excitation will be a $S=1$ spin triplet[4] [for SU(2)], consisting of a confined pair of b_i^α bosons.

2. (π,π) SRO

This state is obtained by quantum disordering the Néel state of Sec. II A 1, and the expectation values of Q_{ij} have the same structure as those in Sec. II A 1. As has been discussed in some detail in Refs. 19 and 20, the quantum fluctuations in this phase are described by a compact U(1) gauge theory. Such a theory is always confining, and thus the b_i^α bosons again bind to yield a $S=1$ quasiparticle above a spin gap. There is also an interesting structure in the spin-singlet sector: This is considered in Sec. III where it is demonstrated that at finite N this phase has ''plaquette'' order.

3. (π,q) and (q,π) SRO

In this phase $\langle Q_{ij}\rangle$ are nonzero on the diagonal, horizontal, and vertical links, like the helical (π,q) LRO phase of Sec. II A 2. Again there are two gauge-nonequivalent configurations, corresponding to the choices $R_1=R_2$ with $Q_i=Q<P_i=P$ [the (π,q) phase] and $R_1=-R_2$ with $Q_i=Q>P_i=P$ [the (q,π) phase]. Thus all of the horizontal Q_i fields acquire the same expectation value, but unlike in the helical LRO phase, this value differs slightly from that of the vertical P_i fields; the difference is only on the order of 1 part in 10 000. The state is a spin singlet and there is a gap to all spin excitations. Nevertheless, the symmetry of 90° rotations between the vertical and horizontal directions is broken—this would now be apparent in various spin-singlet observables like the bond-exchange energies or the bond-charge densities. This phase may therefore be viewed as a spin-singlet ''bond-charge nematic'' as only lattice rotational symmetry is broken (the prefix ''bond charge'' implies that the nematic order is observable only in the charge density in the bonds, which is in turn determined by the magnitude of the spin-singlet exchange energy across the bond). The choice of a vertical or horizontal spatial polarization in the nematic order leads to a twofold degeneracy in the ground state. The state also has ''topological'' order,[25,26,12,24,27,28] and this would lead to an additional fourfold degeneracy in a torus geometry. Unlike the commensurate SRO phases, the spinons are deconfined. We describe the deconfinement transition below in Sec. IV. The spinon dispersion has its minima at momentum $(\pi/2,q/2)$ or $(q/2,\pi/2)$. Although this phase is realized only for $S<1/2$ in the large-N limit, it seems possible that in the physical limit $N=1$ it could extend up to $S=1/2$ for a narrow range of J_2/J_1. Similar behavior was found in a study of the Sp($2N$) Heisenberg antiferromagnet on the anisotropic triangular lattice.[16] It would interesting to search for this phase using numerical methods.

We conclude this section by briefly comparing our results to other published calculations. For $S=1/2$ we find that the transition between Néel and helical LRO phases is continuous, occurring at $J_2/J_1\approx 1.02$, close to the value of 1.1 found by Albrecht and Mila,[5] who also report a continuous transition. Also in agreement with Albrecht and Mila, we find that the transition between the helical LRO and dimer SRO phase is first order, but occurs at $J_2/J_1\approx 2.7$ instead of 1.65. Carpentier and Balents[10] also found a helical LRO phase, but presented arguments that an intermediate phase may exist between the helical LRO and dimer phases: Our (π,q) SRO state is precisely such a phase. Koga and Kawakami[8] employed a series expansion to find, for $S=1/2$, a plaquette phase which intervenes between the Néel and dimer phases. As shown below, the (π,π) SRO phase acquires plaquette order at finite N, but as can be seen in Fig. 3, at large N this phase only occurs for $S<1/5$. If finite-N fluctuations push the phase boundary up to $S=1/2$, then the following sequence of phases would occur as $J_2/(J_1+J_2)$ increases from 0 to 1: Néel, plaquette (π,π) SRO, (π,q) SRO, and finally dimer SRO.

III. PLAQUETTE ORDER IN THE COMMENSURATE PARAMAGNET

This section will discuss the fate of the spin-singlet sector upon including fluctuations about the mean field in the (π,π) SRO state. The results below are a straightforward generalization of those obtained in Refs. 19 and 20 for the square-lattice antiferromagnet. We will only consider the case where $2SN$ is an odd integer [for the physical SU(2) case, this means that S is half an odd integer]; the generalization to other values of S follows as in earlier work.

In the present large-N approach, regular perturbative corrections order by order in $1/N$ do not qualitatively modify the nature of the mean-field ground state. However, singular effects do appear[19,20] upon considering the consequences of ''hedgehog''-like instanton tunneling events and their Berry phases. Such a calculation is technically involved, and a somewhat more transparent discussion of essentially the same physics emerges from studying the ''quantum dimer'' model[25] (see Appendix A of Ref. 20 for a discussion of the equivalence between the instanton physics of the large-N expansion and dual representations of the quantum dimer model). Here we shall follow the treatment of Ref. 29.

The quantum dimer model represents the Hilbert space of low-lying singlet excitations by assuming that it can be mapped onto states represented by a near-neighbor singlet bond (''dimers'') covering of the lattice. In the present (π,π) SRO phase, we need only take dimers connecting nearest-neighbor sites on horizontal and vertical links. The dimers along the diagonal links are assumed to occur only rarely in this phase: They can therefore be integrated out and serve mainly to modify the effective Hamiltonian in the space of horizontal and vertical dimers. Indeed, the most important consequence of this procedure is apparent from a glance at Fig. 1: The diagonal dimers divide the plaquettes of the square lattice into two classes, those with and without diagonal links across them, and we expect dimer resonance terms around these plaquettes to have distinct matrix elements (see Fig. 4). This distinction will be the only difference from earlier analyses,[19,20] and we will show that it is sufficient to lead to plaquette order in the (π,π) SRO phase.

Our results emerge from an analysis of the ''height'' representation of the quantum dimer model.[20,30,31,29,28] There is a rigorous, one-to-one mapping between the set of coverings of the square lattice with nearest-neighbor horizontal and vertical dimers, and the configurations of an interface of heights h_a defined on the sites a of the dual square lattice (we identify two interfaces as equivalent if they are related

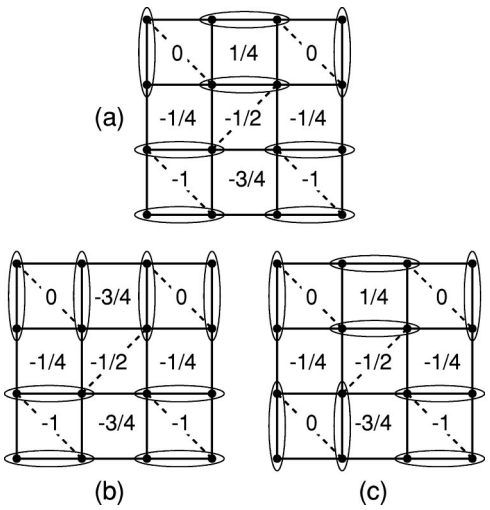

FIG. 4. Three states of the Hilbert space of the quantum dimer model. There are off-diagonal matrix elements in the effective Hamiltonian which connect state (a) to state (b), and state (a) to state (c), by a resonance between pairs of horizontal and vertical dimers around a plaquette. The latter matrix element differs from the former because only the latter has a diagonal link across the resonating plaquette. Also shown are the corresponding values of the heights h_a on the sites of the dual lattice.

by a uniform translation $h_a \rightarrow h_a + p$, where p is any integer). The values of h_a are restricted to

$$h_a = n_a + \zeta_a , \tag{3.1}$$

where n_a is a integer which fluctuates from site to site and ζ_a is a fixed fractional offset which takes the values 0,1/4,1/2,3/4 on four dual sublattices, X,Y,Z,W, as shown in Fig. 5. We further restrict the h_a to satisfy $|h_a - h_b| < 1$ for any pair of nearest-neighbor sites a,b. We can now specify the connection between the height model and the dimer coverings. Examine the value of $|h_a - h_b|$ for every nearest-neighbor pair, and if $|h_a - h_b| > 1/2$, place a dimer on link shared by the plaquettes of the direct lattice around a and b. It is not difficult to see that a consequence of our choice of the ζ_a offsets is that dimers so obtained will form a close-packed covering of the lattice. Examples of the relationship between the height values and dimer coverings are shown in Fig. 4.

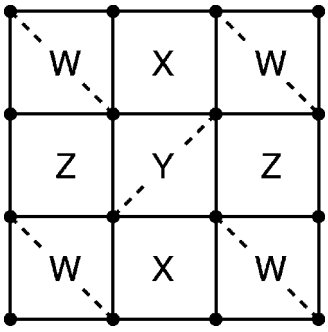

FIG. 5. The four dual sublattices upon which the height offsets take the values $\zeta_W = 0$, $\zeta_X = 1/4$, $\zeta_Y = 1/2$, and $\zeta_Z = 3/4$.

We can now use general symmetry considerations to write down an effective action for the height degrees of freedom. As is standard in theories of interface models, we promote discrete heights h_a, in Eq. (3.1), to continuous real variables χ_a by the Poisson summation formula and ''soften'' the constraints to periodic cosine potentials which have minima at the values $\chi_a = h_a$ which obey Eq. (3.1). In this manner we obtain the action

$$\mathcal{S}_\chi = \int d\tau \left[\frac{K}{2} \sum_{\langle ab \rangle} (\chi_a - \chi_b)^2 + \sum_a \left\{ \frac{K_\tau}{2} (\partial_\tau \chi_a)^2 - y_a \cos[2\pi(\chi_a - \zeta_a)] \right\} \right], \tag{3.2}$$

where the sum over $\langle ab \rangle$ extends over nearest-neighbor sites and K is the stiffness towards spatial fluctuations of the interface height. The corresponding stiffness towards time-dependent fluctuations is K_τ, and, for simplicity, we have taken its value a as independent. The symmetry of the lattice requires that the strength of the periodic potential take two possible values $y_a = y_1$ or $y_a = y_2$ depending upon whether the plaquette a has a diagonal J_2 link across it or not. This is the sole distinction from the analysis of the square lattice antiferromagnet in Ref. 20, which had $y_1 = y_2$.

The fundamental property of interface models in 2+1 dimensions, like $\mathcal{S}_\chi$, is that they are always in a smooth phase. This means that the symmetry of height translations is always broken, and $\langle \chi_a \rangle = \langle h_a \rangle$ has some definite value across the entire system. As was argued in Refs. 19 and 20, any such definite value necessarily breaks the lattice symmetry of the underlying antiferromagnet and will lead here to plaquette order.

With the assumption of a smooth interface, the optimal interface configurations can be determine by a simple minimization of $\mathcal{S}_\chi$ by a set of time-independent values of χ_a. We allow for distinct expectation values χ_W, χ_X, χ_Y, and χ_Z on the four dual sublattices. Then the problem reduces to the minimization of the following energy as a function of these four real variables:

$$E_\chi = K[(\chi_X - \chi_W)^2 + (\chi_W - \chi_Y)^2 + (\chi_Y - \chi_Z)^2 + (\chi_Z - \chi_X)^2] - y_1[\cos(2\pi\chi_W) - \cos(2\pi\chi_Y)] - y_2[\sin(2\pi\chi_X) - \sin(2\pi\chi_Z)]. \tag{3.3}$$

This minimization is a straightforward, but somewhat tedious, computation. The present analysis is valid only for small y_1, y_2, and so we analytically determine the minima in power series in $y_{1,2}$. We define

$$\begin{aligned} \chi_W &= \chi_1 + \chi_2 + \chi_3 , \\ \chi_X &= \chi_1 - \chi_2 + \chi_3 , \\ \chi_Y &= \chi_1 + \chi_2 - \chi_3 , \\ \chi_Z &= \chi_1 - \chi_2 - \chi_3 . \end{aligned} \tag{3.4}$$

We find that at the saddle points of E_χ,

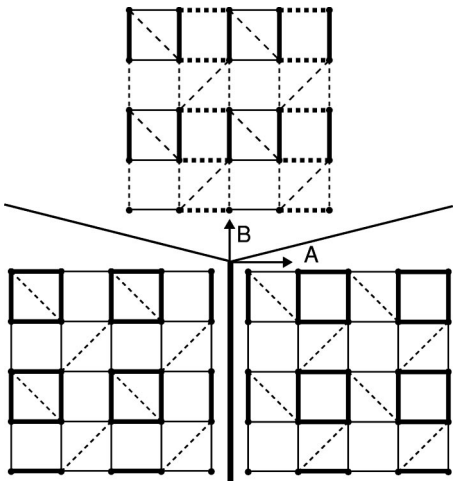

FIG. 6. Phase diagram of Eq. (3.6) as a function of the parameters A and B; this model describes fluctuations in the (π,π) SRO phase of Fig. 3. The thick line is a first-order transition, while the thin lines are second order. The plaquette and spin-Peierls states are shown, with the different line styles representing distinct values of $\langle \mathbf{S}_i \cdot \mathbf{S}_j \rangle$ across the links.

$$\chi_2 = \frac{\pi^3 (y_1^2 + y_2^2)}{16K^2} \sin(4\pi\chi_1) + \mathcal{O}(y_{1,2}^4),$$

$$\chi_3 = -\frac{\pi y_1}{2K} \sin(2\pi\chi_1) + \mathcal{O}(y_{1,2}^3),$$

$$\chi_4 = \frac{\pi y_2}{2K} \cos(2\pi\chi_1) + \mathcal{O}(y_{1,2}^3). \tag{3.5}$$

The average interface height χ_1 is determined by the minimization of

$$E_\chi = E_0 + A\cos(4\pi\chi_1) + B\cos(8\pi\chi_1) + \cdots, \tag{3.6}$$

where E_0 is an uninteresting constant independent of χ_1,

$$A = \frac{\pi^2 (y_1^2 - y_2^2)}{2K} - \frac{\pi^6 (y_1^4 - y_2^4)}{6K^3},$$

$$B = \frac{\pi^6 (7y_1^4 + 6y_1^2 y_2^2 + 7y_2^4)}{96K^3}, \tag{3.7}$$

and all omitted terms are of order $y_{1,2}^6$ or higher [in obtaining the results in Eqs. (3.7) we had to include terms in Eqs. (3.5) which are one order higher than those shown]. Note that the square-lattice antiferromagnet, with $y_1 = y_2$, has $A = 0$.

We now have to minimize Eq. (3.6) to determine χ_1. Then from Eqs. (3.5) we know $\chi_{2,3,4}$, and hence the configuration of the interface heights. Then, from the connection between $|h_a - h_b|$ and the corresponding dimer occupation numbers, we can determine the pattern of the distribution probabilities of the spin-singlet bonds in the original antiferromagnet. It is a simple exercise to determine the minima of Eq. (3.6) for different values of A and B; the resulting phase diagram is shown in Fig. 6, and we now list the various minima and the associated ground states of the antiferromagnet.

(i) $A \geqslant 0$, $B \leqslant A/4$. There are degenerate minima at $\chi_1 = 1/4, 3/4$. The system spontaneously breaks a translational symmetry by choosing one of these minima. With the mappings above, it is easy to see that these are the plaquette states, one of which is depicted in Fig. 6.

(ii) $A \leqslant 0$, $B \leqslant -A/4$. Now the two equivalent minima are $\chi_1 = 0, 1/2$. These also correspond to plaquette states as above, but the chosen plaquettes are now around half of those containing diagonal links (see Fig. 6).

(iii) The remaining values of A and B have four degenerate minima at $\chi_1 = 1/4 \pm \vartheta, 3/4 \pm \vartheta$, where $0 < \vartheta < 1/4$ varies continuously as a function of A/B. These states have spin-Peierls order of the type shown in Fig. 6: The links are divided into four columnar sets, with each set having a different value of $\langle \mathbf{S}_i \cdot \mathbf{S}_j \rangle$ on its links. This state interpolates between the plaquette state in (i) as $\vartheta \to 0$ and that in (ii) as $\vartheta \to 1/4$.

The present analysis is for small y_1, and so, from Eqs. (3.7) we should assume that $B \ll |A|$. Furthermore, the presence of the frustrating J_2 interaction on half the plaquettes means that the hedgehog tunneling events are more likely to be centered on these plaquettes. Using the mapping of such events to the model (3.2), we expect that $y_1 > y_2$. From Eqs. (3.7) we therefore conclude that the most likely possibility for the ground state is that in (i) above. The same state has also been considered in Ref. 8.

We conclude this section with a few comments on the (π,π) SRO phase of the antiferromagnet with full square-lattice symmetry, in which there is a diagonal J_2 exchange between every pair of next-nearest-neighbor sites. Recent numerical work on such an antiferromagnet[32,18] has found evidence for spin-Peierls ordering with the same spatial structure as in (iii) above for the Shastry-Sutherland antiferromagnet. However, we noted earlier that the square-lattice symmetry implies that $A = 0$: For this value, $\vartheta = 1/8$, and the spin-Peierls state of (iii) has a larger symmetry (two of the four sets of columnar links are equal to each other) and becomes equivalent to the ordering discussed in Refs. 19 and 20. To obtain $\vartheta \neq 1/8$, and so a ground state with the symmetry of that in Fig. 6, we need to add to E_χ a higher-order term $C\cos(16\pi\chi)$: Then there can be an *eightfold* degenerate ground state, with ϑ and $1/4 - \vartheta$ equivalent to each other. This is the state that appears to have been found in Refs. 32 and 18.

Note also that for the square-lattice case, the $B < 0$, $A = 0$ solution has the four plaquette states degenerate with each other.[29]

IV. DECONFINEMENT TRANSITION OF THE DIMER PHASE

The deconfined, ''spin-liquid,'' (π,q) SRO phase in Fig. 3 is flanked on both sides by confining paramagnetic phases: the plaquette and dimer phases.

As we indicated Sec. I, the deconfinement-confinement quantum phase transition from the (π,q) SRO phase to the plaquette phase can be described in a theory essentially identical to that considered previously for frustrated square-

lattice antiferromagnets.[12,14] At the mean-field level, the transition is signaled by the onset of nonzero expectation values of Q_{ij} on the diagonal links: We will denote these diagonal Q_{ij} as Q_{ij}^d. Upon considering fluctuations, we find that the Q_{ij}^d constitute a charge-2 Higgs field in a compact U(1) gauge theory, and the deconfinment-confinement transition is that in a Z_2 gauge theory.[21,12–14,22–24]

This section will consider the second deconfinement-confinement transition in Fig. 3 between the dimer and (π,q) SRO phases in more detail. We will see that this is also described by a Z_2 gauge theory, and the emergence of the Z_2 gauge symmetry can be described in a somewhat more transparent manner.

As noted in Sec. II B 1, the dimer phase is characterized by nonzero expectation values of the diagonal Q_{ij}^d links. These links are all decoupled from each other, and this leads to a simple, local structure in the effective action for the fluctuations. The transition to the deconfined phase is now signaled by the onset of nonzero expectation values of the Q_{ij} on the horizontal and vertical links, and we will denote these by Q_{ij}^h and Q_{ij}^v, respectively. Near the phase boundary, we need only consider the structure of the effective action as a functional of the $Q_{ij}^{h,v}$ after all other degrees of freedom have been integrated out.

The simplest terms in the effective action arise from the on-site propagation of the b_i^α on the site i in imaginary time. Integrating out the b_i^α in powers of the $Q_{ij}^{h,v}$, the lowest-order terms have the form

$$\mathcal{S}_1 = \int d\tau \Bigg[c_1 \sum_{\langle ij \rangle} |Q_{ij}^{h,v}|^2 + c_2 \sum_{\square} \{Q_{12}^h Q_{23}^{v*} Q_{34}^h Q_{41}^{v*} + \text{H.c.}\} + \cdots \Bigg], \tag{4.1}$$

where c_1, c_2 are constants, the first sum is over nearest-neighbor links, and the second sum is over plaquettes, with the sites labeled as in Fig. 7. A crucial property of $\mathcal{S}_1$ is that all terms are invariant under a local U(1) gauge transformation

$$Q_{ij}^{h,v} \to Q_{ij}^{h,v} e^{i(\phi_i + \phi_j)}, \tag{4.2}$$

where the phase ϕ_i can take arbitrary distinct values on the sites i.

We have so far not made use of the fact that the nonzero value of $\langle Q_{ij}^d \rangle$ allows the b_i^α bosons to hop across a single diagonal link. Such hopping processes will induce a large number of additional terms between the $Q_{ij}^{h,v}$. We will now write down the structure of all such terms which appear at fourth order in the $Q_{ij}^{h,v}$. It is convenient to group these terms into sets associated with links emanating from a given plaquette which does not have a diagonal dimer across it: One such plaquette is that with the sites 1,2,3,4 in Fig. 7, and we now write down all four-link terms in which every link has at least one site on the central plaquette. It is not difficult to see that all other four-link terms can be obtained by a simple translation of these terms to other plaquettes. The terms are

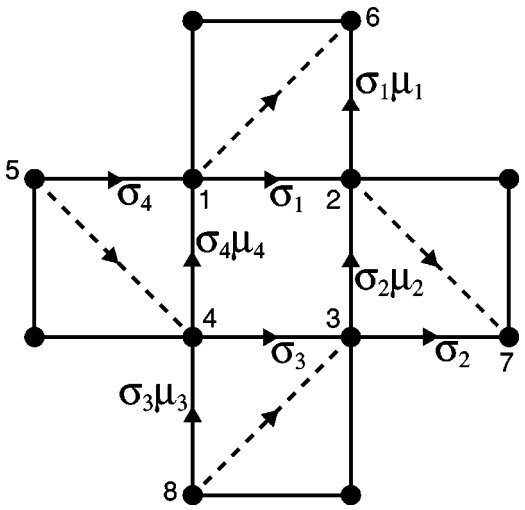

FIG. 7. A section of the Shastry-Sutherland lattice. We have labeled sites around the central plaquette to enable the discussion in Sec. IV of the various terms in the Z_2 gauge theory of the transition from the dimer state to the (π,q) SRO phase with spinon deconfinement.

$$\begin{aligned}\mathcal{S}_2 = \int d\tau [& c_3 \{ Q_{51}^h Q_{26}^v Q_{32}^{v*} Q_{43}^h - Q_{26}^v Q_{37}^h Q_{43}^{h*} Q_{41}^v \\ & + Q_{37}^h Q_{84}^v Q_{41}^{v*} Q_{12}^h - Q_{84}^v Q_{51}^h Q_{12}^{h*} Q_{32}^v + \text{c.c.} \} \\ & + c_4 \{ Q_{51}^h Q_{26}^v Q_{12}^{h*} Q_{41}^v - Q_{26}^v Q_{37}^h Q_{32}^{v*} Q_{12}^h \\ & + Q_{37}^h Q_{84}^v Q_{43}^{h*} Q_{32}^v - Q_{84}^v Q_{51}^h Q_{41}^{v*} Q_{43}^h + \text{c.c.} \} \\ & - c_5 \{ Q_{51}^h Q_{12}^{h*} Q_{37}^{h*} Q_{43}^h + Q_{26}^v Q_{32}^{v*} Q_{84}^{v*} Q_{41}^v + \text{c.c.} \} \\ & + c_6 \{ Q_{51}^h Q_{26}^v Q_{37}^h Q_{84}^v + \text{c.c.} \}]. \end{aligned} \tag{4.3}$$

Clearly, Eq. (4.3) is not invariant under Eq. (4.2). However, a residual Z_2 gauge symmetry does survive. We see that Eqs. (4.1) and (4.3), and all other allowed terms, are invariant under

$$Q_{ij}^{h,v} \to Q_{ij}^{h,v} \eta_i \eta_j, \tag{4.4}$$

where $\eta_i = \pm 1$ performs the gauge transformation. However, it is *not* possible to choose the η_i independently on every site: It is easy to see that we need the additional constraint

$$\eta_i = \eta_j \text{ whenever } i \text{ and } j \text{ are separated by a diagonal link.} \tag{4.5}$$

So the Z_2 gauge degree of freedom is halved from that present on the original square lattice.

To place the Z_2 gauge theory in a more conventional form, it is useful to introduce a slightly different parametrization of the degrees of freedom. First, we neglect all amplitude and phase fluctuations and replace all the Q_{ij} by discrete Ising variables taking only the values ± 1. Then we choose to represent all the Q_{ij}^h as Ising gauge fields σ, while all the Q_{ij}^v are written as products of σ and a second Ising spin field μ; thus,

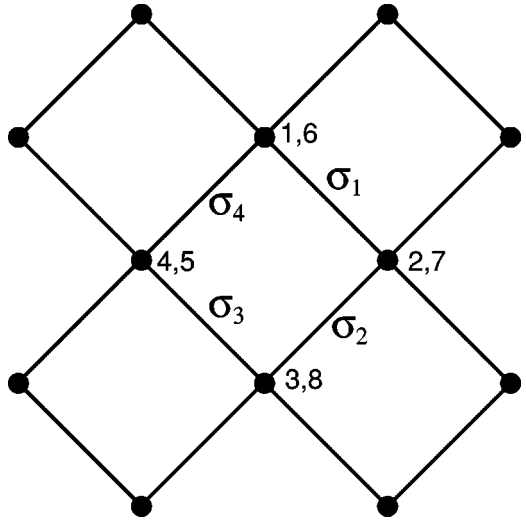

FIG. 8. A deformation of the Shastry-Sutherland lattice which exposes the structure of the Z_2 gauge theory. Pairs of sites across a diagonal bond have been compressed into a single site. Four of the sites carry pairs of sites labels, corresponding to the original site numbers in Fig. 7. The Z_2 Ising gauge fields on some of the links are indicated, with a notation corresponding to the degrees of freedom in Fig. 7.

$$Q^h \sim \sigma,$$

$$Q^v \sim \sigma\mu. \tag{4.6}$$

This is shown a more explicitly in Fig. 7. Notice that each pair of horizontal and vertical links that form a triangle with a single diagonal link shares the same Ising gauge field σ. This choice is a consequence of the constraint (4.5)—as a result, all the μ fields are *invariant* under the gauge transformation generated by the η_i, while the σ's transform like conventional Ising gauge fields. This is also evident from the structure of the effective action obtained by substituting the parametrization in Eq. (4.6) and Fig. 7 into the effective action in Eqs. (4.1) and (4.3); for the terms displayed in Eqs. (4.1) and (4.3) we obtain

$$\begin{aligned}\mathcal{S}_3 = \int d\tau [& \tilde{c}_2 \sigma_1\sigma_2\sigma_3\sigma_4\mu_2\mu_4 + \tilde{c}_3 \sigma_1\sigma_2\sigma_3\sigma_4\{\mu_1\mu_2 - \mu_1\mu_4 \\ & + \mu_3\mu_4 - \mu_3\mu_2\} + \tilde{c}_4\{\mu_1\mu_4 - \mu_1\mu_2 + \mu_2\mu_3 - \mu_3\mu_4\} \\ & - \tilde{c}_5 \sigma_1\sigma_2\sigma_3\sigma_4\{1 + \mu_1\mu_2\mu_3\mu_4\} + \tilde{c}_6 \sigma_1\sigma_2\sigma_3\sigma_4\mu_1\mu_3].\end{aligned} \tag{4.7}$$

The terms involving the σ_i appear to have the plaquette form associated with Ising gauge fields. The spatial structure of these gauge interactions is made clearer by the transformation in Fig. 8. Here, we have collapsed pairs of sites connected by the diagonal links into single sites—we now see that the σ_i can viewed as residing on the links of a square lattice which is tilted by 45° from the original lattice, and their gauge interactions have the usual form around elementary plaquettes.

The μ_i constitute a separate global Ising degree of freedom associated with the breaking of the symmetry of 90° spatial rotations between the horizontal and vertical directions. In the mean-field theory of the deconfined phase, the state with $\mu_i = 1$ corresponds to the state with dominant spin correlations at the wave vector (π, q) (say). The degenerate partner state with spin correlations at (q, π) is obtained by the state $\mu_i = (-1)^{i_y}$, where (i_x, i_y) are the Cartesian coordinates of the site i.

So the action $\mathcal{S}_3$ describes a Z_2 gauge theory (σ) coupled (rather intricately) to an Ising spin field (μ); the μ field does not carry a nonzero charge under the Z_2 gauge transformation. The Z_2 gauge theory can undergo a confinement-deconfinement transition (which is related by a duality transformation to the magnetic transition in an Ising model in three dimensions), corresponding to the liberation of spinons upon moving out of the dimer phase. In a different sector, the ordering of the μ degrees of freedom leads to the appearance of bond charge nematic order and the breaking of the symmetry of 90° spatial rotations. In the mean-field theory, these two transitions occur at the same point; i.e., the deconfinement transition is also the point where the spatial rotation symmetry is broken. More generally, the interplay between these two potentially distinct transitions can be addressed by an analysis of fluctuations using the action $\mathcal{S}_3$. It does appear possible that the two transitions are not simultaneous and that there can be a deconfined phase without any broken spatial symmetries; moreover, if there is a simultaneous transition in the two sectors, it is likely to be first order. A more definitive conclusion on these issues must await a complete study of the coupled Ising gauge and Ising spin theory defined by $\mathcal{S}_3$. We note that these issues concerning the transition from the confined dimer phase to the deconfined helical SRO phase are somewhat different from earlier deconfinement transitions[23] because here the dimer phase does not break any lattice symmetries.

V. CONCLUSIONS

The Mott insulator $SrCu_2(BO_3)_2$ is perhaps the only experimental example of a spin-gap paramagnet on a strongly frustrated two-dimensional lattice. Another experimental example of a two-dimensional paramagnet is CaV_4O_9, but its spin gap is realized by homogeneous dilution and modulation of the exchange constants, not frustration. A spin-gap state is also expected on the $S = 1/2$ *kagomé* lattice antiferromagnet: In Ref. 15 this state was described by a theory very similar to that discussed here for the (π, q) SRO phase, with deconfined spinons and topological order. (It is known numerically that the *kagomé* antiferromagnet also has a large density of low-energy singlet excitations—in the present theory these singlet modes are captured by the gauge fluctuations and are eventually expected to acquire a small, but finite, singlet gap.[33,15,34–36]) However, thus far there have been no well-characterized experimental examples of the $S = 1/2$ *kagomé* antiferromagnet.

To date, it appears that the spin gap in $SrCu_2(BO_3)_2$ is realized in a simple decoupled dimer ground state discovered originally by Shastry and Sutherland.[3] Here, we undertook a

more detailed study of the parameter space of this antiferromagnet and found that other paramagnetic spin-gap states are also possible. One of these was the plaquette state,[8] which appears in a region of weaker frustration and commensurate spin correlations. The other was a more exotic state with ''topological order,'' deconfined $S=1/2$ excitations, and helical spin correlations. The latter state was found to be contiguous to the dimer state and so not too far from the physically relevant regime: It appears that $SrCu_2(BO_3)_2$ is quite close to the boundary of stability of the dimer phase.

Our results suggest exciting possibilities for materials obtained by doping $SrCu_2(BO_3)_2$ with mobile carriers. It is expected that the helical state will be more amenable to the motion of charge carriers than the dimer state, and so doping may well drive the system into a topologically ordered state. Such a state is a prime candidate for superconductivity with the exotic properties associated with the proximity of a Mott insulator with deconfined spinons: These include a regime of stable hc/e vortices[37,38] and the closely related flux-trapping effect of Senthil and Fisher.[39] An experimental effort to dope $SrCu_2(BO_3)_2$ (or related compounds) therefore appears worthwhile.

ACKNOWLEDGMENTS

This research was supported by U.S. NSF Grant Nos. DMR 00-98226 (S.S.) and DMR 97-12391 (J.B.M.).

APPENDIX

This appendix will provide a proof of a statement made in Sec. II A 2 on the nature of the saddle point in the phase with helical LRO: We will analytically show that in the (π,q) and (q,π) LRO phases the link fields obey the following relations:

$$Q=P,$$

$$|R_1|=|R_2|, \tag{A1}$$

where $|Q_i|=Q$, $|P_i|=P$. The reasoning is the same in the both (π,q) and (q,π) phases, and we will fix our state in the (π,q) phase for simplicity. In this state, the directions of the link fields Q_{ij} are shown as in Fig. 2. The spinon dispersion in this phase can be obtained from the following eigenvalue equation[15] in momentum space:

$$\tau^3 D(k) M = M \tau^3 \hat{\omega}(k),$$

$$\tau^3 = \begin{pmatrix} ¶ & 0 \\ 0 & -¶ \end{pmatrix},$$

$$D(k) = \begin{pmatrix} \lambda ¶ & P(k) \\ P^{\dagger}(k) & \lambda ¶ \end{pmatrix}, \tag{A2}$$

where ¶ is the 4×4 unit matrix, $\hat{\omega}(k)$ is a diagonal matrix of the bosonic eigenenergies, M is a 8×8 matrix whose columns are the eigenvectors of the matrix $\tau^3 D(k)$, and the diagonal elements of $\tau^3\hat{\omega}(k)$ are the corresponding eigenvalues; $P(k)$ is a 4×4 matrix with the following form:

$$P(k) = \begin{pmatrix} 0 & iJ_1 Q \sin(k_x) & (J_2 R_1/2) e^{i(k_x - k_y)} & iJ_1 P \sin(k_y) \\ iJ_1 Q \sin(k_x) & 0 & (J_2 R_2/2) e^{i(k_x + k_y)} & \\ -(J_2 R_1/2) e^{-i(k_x - k_y)} & iJ_1 P \sin(k_y) & 0 & iJ_1 Q \sin(k_x) \\ iJ_1 P \sin(k_y) & -(J_2 R_2/2) e^{-i(k_x + k_y)} & iJ_1 Q \sin(k_x) & 0 \end{pmatrix}, \tag{A3}$$

and λ is the Largrange multiplier of the mean-field Hamiltonian which we assume to be independent of lattice site i. With this assumption, it can be shown[15] that the eigenvalues occur in pairs with opposite signs $(\omega_\mu(k), -\omega_\mu(k))$ where $\mu=1,\ldots,4$, and the matrix M has the form

$$M = \begin{pmatrix} U & -V^* \\ V & U^* \end{pmatrix}, \tag{A4}$$

where the U, V are 4×4 matrices associated with the positive eigenvalues. The (π,q) LRO phase $(x_i^\alpha \neq 0)$ occurs at the wave vector $\vec{k}_{min}=(\pm\pi/2,\pm q/2)$ where the eigenenergy vanishes, i.e., $\omega(\vec{k}_{min})=0$. The two linearly independent eigenvectors associated with $\vec{k}_1=(\pi/2,q/2)$ and $\vec{k}_2=(\pi/2,-q/2)$ can be shown to be

$$\Psi_1 = (1, ie^{-iq/2}, ie^{-iq/2}, 1, i, -e^{-iq/2}, -e^{-iq/2}, i) e^{i\vec{k}_1\cdot\vec{r}},$$

$$\Psi_2 = (1, ie^{iq/2}, ie^{iq/2}, 1, -i, e^{iq/2}, e^{iq/2}, -i) e^{i\vec{k}_2\cdot\vec{r}}, \tag{A5}$$

respectively. Substituting Ψ_1 (or Ψ_2) into Eq. (A2), we have

$$\lambda - \left[J_1 (P+Q) \sin(q/2) + J_2 \frac{R_1}{2} \sin(q) \right]$$

$$+ i \left[J_1 Q \cos(q/2) + J_2 \frac{R_1}{2} \cos(q) \right] = 0,$$

$$\lambda - \left[J_1(P+Q)\sin(q/2) + J_2 \frac{R_2}{2}\sin(q) \right]$$

$$+ i\left[J_1 Q \cos(q/2) + J_2 \frac{R_2}{2}\cos(q) \right] = 0. \quad \text{(A6)}$$

We can easily see that $R_1 = R_2 = R$ from the above conditions. Also, we find that each saddle point may be described by purely real $\langle Q_{ij} \rangle$. Therefore, we may fix the values of λ and q in the LRO phase from the above condition:

$$J_1(P+Q)\sin(q/2) + J_2 \frac{R}{2}\sin(q) = \lambda,$$

$$J_1 Q \cos(q/2) + J_2 \frac{R}{2}\cos(q) = 0. \quad \text{(A7)}$$

To prove $P = Q$, we need one additional condition from the saddle-point equations. The mean-field free energy E_{MF} is a function of λ, Q, P, R, and $x^{\alpha}(q)$ where these are independent parameters. The large-N solutions of this model are obtained by solving the saddle-point equations which set the derivatives of free energy with respect to these independent variables to be zero. Notice that q is also an independent parameter. The additional condition we need comes from the saddle-point equation associated with q. It is given by

$$\frac{\partial E_{MF}}{\partial q} = 0. \quad \text{(A8)}$$

The only explicit q dependence in the free energy is in the Bose condensate variables $x^{\alpha}(q)$. This piece of free energy is given by[15]

$$E_x(q) = \sum_{i>j} \frac{J_{ij}}{2} [- Q_{ij} \epsilon_{\sigma\sigma'} x_i^{\sigma}(q) x_j^{\sigma'}(q) + \text{H.c.}], \quad \text{(A9)}$$

where $\epsilon_{\sigma\sigma'}$ is the SU(2) antisymmetric ϵ tensor, and $\sigma, \sigma' = \uparrow, \downarrow$. The condensates $x_i^{\sigma}(q)$ must be the linear combinations of the eigenvectors Ψ_1 and Ψ_2 associated with the zero mode: this introduces two complex numbers c_1, c_2, with only the value of $|c_1|^2 + |c_2|^2$ fixed by the saddle-point equations.[15] Working out the orientation of the condensate at every lattice site over the unit cell, the condensates can be written in the form

$$\begin{pmatrix} x_A^{\uparrow} \\ x_A^{\downarrow} \end{pmatrix} = \begin{pmatrix} c_1 + c_2 \\ i c_2^* - i c_1^* \end{pmatrix},$$

$$\begin{pmatrix} x_B^{\uparrow} \\ x_B^{\downarrow} \end{pmatrix} = \begin{pmatrix} -c_1 e^{-iq/2} - c_2 e^{iq/2} \\ -i c_2^* e^{-iq/2} + i c_1^* e^{iq/2} \end{pmatrix},$$

$$\begin{pmatrix} x_C^{\uparrow} \\ x_C^{\downarrow} \end{pmatrix} = \begin{pmatrix} -c_1 e^{-iq} - c_2 e^{iq} \\ -i c_2^* e^{-iq} - i c_1^* e^{iq} \end{pmatrix},$$

$$\begin{pmatrix} x_D^{\uparrow} \\ x_D^{\downarrow} \end{pmatrix} = \begin{pmatrix} c_1 e^{-iq/2} + c_2 e^{iq/2} \\ i c_2^* e^{-iq/2} - i c_1^* e^{iq/2} \end{pmatrix}. \quad \text{(A10)}$$

By substituting Eqs. (A10) into Eq. (A9), we can explicitly work out $E_x(q)$. It is given by

$$E_x(q) = -\left[J_1(P+Q)\sin(q/2) + J_2 \frac{R}{2}\sin(q) \right] (|c_1|^2 + |c_2|^2). \quad \text{(A11)}$$

Now the saddle-point condition (A8) becomes

$$\frac{\partial E_{MF}}{\partial q} = J_1 \frac{P+Q}{2}\cos(q/2) + J_2 \frac{R}{2}\cos(q) = 0. \quad \text{(A12)}$$

Combining Eqs. (A7) and (A12), we have $P = Q$.

[1] H. Kageyama, K. Yoshimura, R. Stern, N.V. Mushnikov, K. Onizuka, M. Kato, K. Kosuge, C.P. Slichter, T. Goto, and Y. Ueda, Phys. Rev. Lett. **82**, 3168 (1999).
[2] H. Kageyama, M. Nishi, N. Aso, K. Onizuka, T. Yosihama, K. Nukui, K. Kodama, K. Kakurai, and Y. Ueda, Phys. Rev. Lett. **84**, 5876 (2000).
[3] B.S. Shastry and B. Sutherland, Physica B **108**, 1069 (1981).
[4] S. Miyahara and K. Ueda, Phys. Rev. Lett. **82**, 3701 (1999).
[5] M. Albrecht and F. Mila, Europhys. Lett. **34**, 145 (1996).
[6] Zheng Weihong, C.J. Hamer, and J. Oitmaa, Phys. Rev. B **60**, 6608 (1999).
[7] E. Müller-Hartmann, R.R.P. Singh, C. Knetter and G.S. Uhrig, Phys. Rev. Lett. **84**, 1808 (2000).
[8] A. Koga and N. Kawakami, Phys. Rev. Lett. **84**, 4461 (2000).
[9] C. Knetter, A. Bühler, E. Müller-Hartmann, and G.S. Uhrig, Phys. Rev. Lett. **85**, 3958 (2000).
[10] D. Carpentier and L. Balents, cond-mat/0102218 (unpublished).
[11] G. Misguich, Th. Jolicoeur, and S.M. Girvin, cond-mat/0102377 (unpublished).
[12] N. Read and S. Sachdev, Phys. Rev. Lett. **66**, 1773 (1991).
[13] R.A. Jalabert and S. Sachdev, Phys. Rev. B **44**, 686 (1991).
[14] S. Sachdev and N. Read, Int. J. Mod. Phys. B **5**, 219 (1991).
[15] S. Sachdev, Phys. Rev. B **45**, 12 377 (1992).
[16] C.H. Chung, J.B. Marston, and R.H. McKenzie, J. Phys.: Condens. Matter **13**, 5159 (2001).
[17] S. Sachdev and R. Jalabert, Mod. Phys. Lett. B **4**, 1043 (1990).
[18] O.P. Sushkov, J. Oitmaa, and Z. Weihong, Phys. Rev. B **63**, 104420 (2001).
[19] N. Read and S. Sachdev, Phys. Rev. Lett. **62**, 1694 (1989).
[20] N. Read and S. Sachdev, Phys. Rev. B **42**, 4568 (1990).
[21] E. Fradkin and S.H. Shenker, Phys. Rev. D **19**, 3682 (1976).
[22] X.G. Wen, Phys. Rev. B **44**, 2664 (1991).
[23] S. Sachdev and M. Vojta, J. Phys. Soc. Jpn. **69**, 1 (2000).
[24] T. Senthil and M.P.A. Fisher, Phys. Rev. B **62**, 7850 (2000).
[25] D.S. Rokhsar and S.A. Kivelson, Phys. Rev. Lett. **61**, 2376 (1988).
[26] N. Read and B. Chakraborty, Phys. Rev. B **40**, 7133 (1989).
[27] G. Misguich and C. Lhuillier, cond-mat/0002170 (unpublished).
[28] R. Moessner and S.L. Sondhi, Phys. Rev. Lett. **86**, 1881 (2001).
[29] S. Sachdev and N. Read, Phys. Rev. Lett. **77**, 4800 (1996).

[30] E. Fradkin and S. Kivelson, Mod. Phys. Lett. B **4**, 229 (1990).
[31] W. Zheng and S. Sachdev, Phys. Rev. B **40**, 2704 (1989).
[32] M.S.L. du Croo de Jongh, J.M.J. van Leeuwen, and W. van Saarloos, Phys. Rev. B **62**, 14 844 (2000).
[33] J.B. Marston and C. Zeng, J. Appl. Phys. **69**, 5962 (1991).
[34] S.R. White and R.R.P. Singh, Phys. Rev. Lett. **85**, 3330 (2000).
[35] M.B. Hastings, Phys. Rev. B **63**, 014413 (2001).
[36] R. Siddharthan and A. Georges, cond-mat/0103334 (unpublished).
[37] S. Sachdev, Phys. Rev. B **45**, 389 (1992).
[38] N. Nagaosa and P.A. Lee, Phys. Rev. B **45**, 966 (1992).
[39] T. Senthil and M.P.A. Fisher, Phys. Rev. Lett. **86**, 292 (2001).